

Central engine of a gamma-ray blazar resolved through the magnifying glass of gravitational microlensing

Andrii Neronov^{1*}, Ievgen Vovk^{2*} and Denys Malyshev¹

Gamma-ray emission from blazars is known to originate from jets emitted by supermassive black holes¹. However, the exact location and size of the γ -ray emitting part of the jets is uncertain^{2–6}. The main difficulty is the very small angular size of these sources, beyond the angular resolution of γ -ray telescopes. Here, we report a measurement of the projected size of the γ -ray jet, revealed by the detection of microlensing in the gravitationally lensed blazar PKS 1830-211. This measurement is consistent with a constraint from the intrinsic variability timescale of the blazar. Our measurement shows that the γ -ray emission originates from the vicinity of the central supermassive black hole. Combining the X-ray and γ -ray data, we use the microlensing effect to constrain the size of the X-ray source. We show that the effect of pair production of γ -rays on X-ray photons does not make the source opaque, owing to the large size of the X-ray emission region.

Active galactic nuclei (AGN) emitting relativistic jets aligned along the line of sight, known as blazars¹, dominate the extragalactic γ -ray sky⁷. Observations of fast variability of the γ -ray flux^{2,3} indicate that sites of the γ -ray emission are probably situated not far away from their supermassive black hole ‘central engine’. However, the interaction of γ -rays with the dense soft background photons⁸ produced by the jet⁹ or by the accretion flow^{10,11}, and subsequently scattered in the broad line region^{12,13}, should prevent the escape of γ -rays from the central engine. A possible solution to this problem is to assume that the γ -rays come from a larger, parsec-scale region, where the density of the soft photon backgrounds is low enough to allow escape of the high-energy photons^{4–6}. In such a scenario, the fast variability of the γ -ray flux is unrelated to the central black hole and has to be attributed to other physical phenomena—for example, to the presence of small inhomogeneities inside the parsec-scale jet^{14–16}.

Central engines of AGN of size $R_{\text{BH}} \simeq 3 \times 10^{14} (M_{\text{BH}}/10^9 M_{\odot}) \text{ cm}$ (M_{BH} is the mass of the black hole) are not directly resolvable by telescopes. Nevertheless, observations in the visible band do manage to extract information on the central engines of gravitationally lensed AGN, using the effect of microlensing^{17–21}. This effect is due to stars in the intervening galaxy that act as a natural ‘magnifying glass’, selectively magnifying the flux from sub-structures with sizes smaller than the size of the Einstein ring $R_E^* \simeq 4 \times 10^{16} (M_*/M_{\odot})^{1/2} \text{ cm}$ (M_* is the mass of the lensing star).

Here we report detection of the microlensing of the blazar PKS 1830-211. We further use this detection to measure the size of the X- and γ -ray emitting parts of its jet. PKS 1830-211 is a known

gravitationally lensed AGN (ref. 22) at redshift $z_s \simeq 2.5$ (ref. 23), lensed by a face-on spiral galaxy at redshift $z_l \simeq 0.89$ (ref. 24) and, possibly, by another galaxy at redshift $z_{l2} \simeq 0.19$ (ref. 25). The source image consists of an Einstein ring of radius $\theta_E \simeq 0.5''$, on which two images of the source separated by an angular distance $\theta \simeq 2\theta_E$ are superimposed. The ring and the two images are not resolvable by the γ -ray and X-ray telescopes used in our analysis. For this reason both images and the ring contribute to the observed γ - and X-ray fluxes.

The contributions of each of the two images to the overall source flux could be distinguished based on the variability properties of the signal^{26,27}. The gravitational time delay of the source is measured from the observations in the radio band, $\tau_{\text{radio}} \simeq 26^{+4}_{-5} \text{ d}$ (ref. 28). As the gravitational time delay is an achromatic phenomenon, a γ -ray flare of the primary source is expected to produce a double-peak signal in the telescope, with two subsequent flaring episodes of the two images separated by the interval τ_{radio} . The ratio of the peak fluxes of the two flares is equal to the magnification ratio $\mu_{\text{radio}} = 1.52 \pm 0.05$, also known from the radio observations²⁸.

PKS 1830-211 has exhibited several pronounced flares during the six-year observation period by the Large Area Telescope (LAT) on board of the Fermi satellite. The source flux during the flares varied by almost an order of magnitude on timescales of 1–100 d (Fig. 1) in the energy band 0.1–500 GeV. We have searched for the gravitational time delay in the γ -ray signal using structure function and wavelet analysis techniques (see Supplementary Information for details). Both techniques have identified two characteristic timescales, $\tau_{\gamma} = 21^{+2}_{-2} (\text{stat})^{+2}_{-3} (\text{sys}) \text{ d}$ and $\tau_{\text{rep}} = 76^{+7}_{-7} (\text{stat})^{+18}_{-8} (\text{sys}) \text{ d}$, recurrent in all flaring episodes. A recent paper²⁷, which appeared during the referring process of this paper, has also identified the timescale of 76 days. The timescale of 19 d, comparable to τ_{γ} , noticed in ref. 27, was considered to be not significant. Our analysis is based on six years of data (compared to a three-year period in ref. 27) and higher-quality Pass 7 event selection (compared to Pass 6 in ref. 27) with a lower energy threshold. Repeating the wavelet timing analysis of ref. 27 with our data set, we detect the timescale τ_{γ} with significance 5.2σ (see Supplementary Information for details).

τ_{γ} can be identified with the gravitational time delay measured in the radio band. An alternative possibility of identification of the time delay with τ_{rep} is inconsistent with the radio data²⁸ at more than 5σ level (see Supplementary Information for details). Detection of the gravitational time delay allows a measurement of the magnification factor ratio $\mu_{\gamma} = 3.1 \pm 0.5$, averaged over all detected flares. This value of μ_{γ} is not consistent with μ_{radio} . Moreover, μ_{γ} seems to be variable in the range $\mu_{\gamma} \sim 2$ –7 from flare to flare (with a chance probability of 0.7%, see Supplementary Information).

¹ISDC, Astronomy Department, University of Geneva, Ch. d’Ecogia 16, Versoix 1290, Switzerland. ²Max Planck Institut für Physik, Föhringer Ring 6, München 80805, Germany. *e-mail: Andrii.Neronov@unige.ch; ie.vovk@mpp.mpg.de

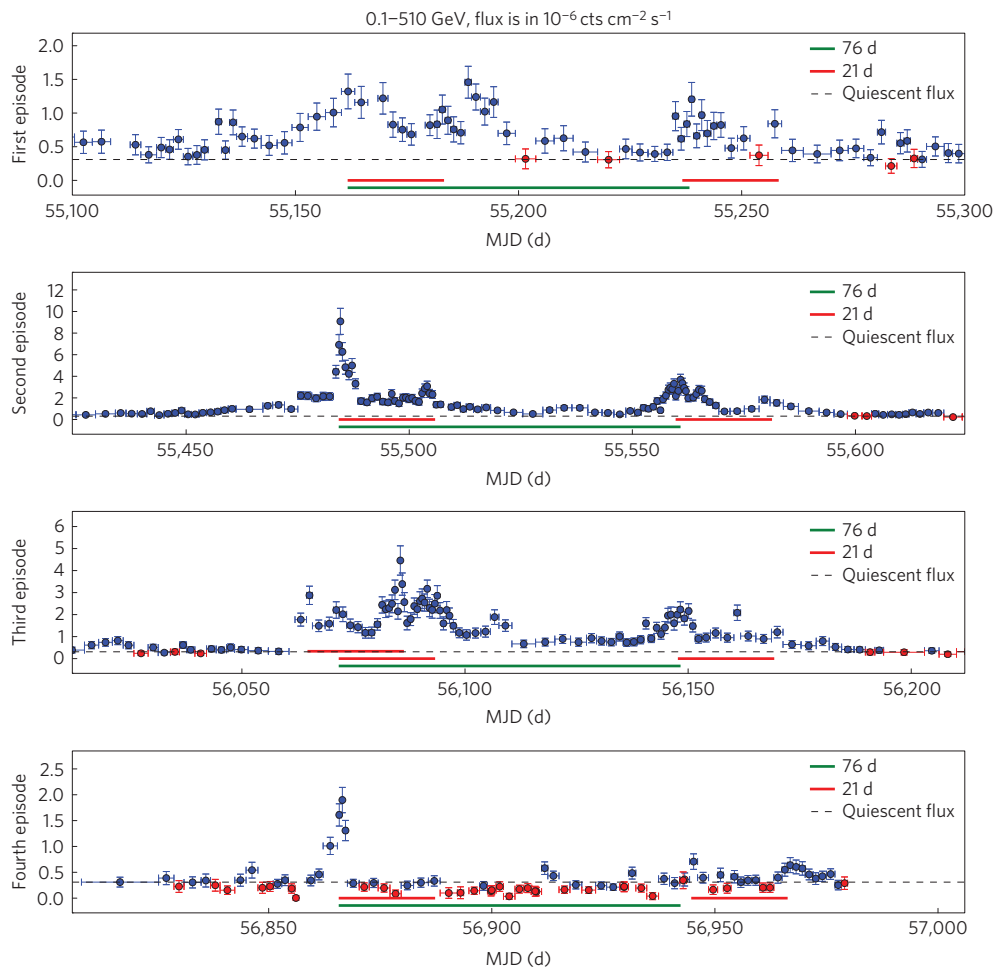


Figure 1 | Fermi/LAT light curves of PKS 1830-211 over the flaring episodes, produced with adaptive time binning. The error bars are 68% confidence intervals computed using the likelihood analysis (see Supplementary Information for details). The data points marked with red represent the time bins with significance of detection less than 3σ . The quiescent flux of the source, determined over the time period MJD 56,300–56,700 (between the third and fourth flaring episodes) using only the data points with significant detection, is indicated by the horizontal dashed line. The characteristic timescales identified from the structure function analysis— ~ 21 d and ~ 76 d—are marked with red and green horizontal bands.

The difference in the magnification factor ratios between radio and γ -ray emission, as well as from flare to flare, can be consistently explained as an effect of the gravitational microlensing^{17–21}. Microlensing does not affect μ_{radio} because the radio emission comes from the parsec-scale jet—that is, from a source which is much larger than R_E^* . Instead, the microlensing affects only the flux of the γ -ray source, if its size is comparable or smaller than R_E^* .

The maximum magnification of the source flux due to microlensing occurs during the caustic crossing events. It is determined by the ratio of the size of the γ -ray source, R_γ , and R_E^* , $\mu_\gamma \leq \mu_{\text{radio}}(R_E^*/R_\gamma)^{1/2}$ (ref. 29). The observed values in the range $\mu_\gamma \sim 2$ –7 can be achieved if the γ -ray source is extremely compact, $R_\gamma \lesssim 0.1R_E^* \sim 2 \times 10^{15}(M_*/M_\odot)^{1/2}$ cm. This qualitative result is confirmed by numerical simulation of the caustic crossing events (see Supplementary Information for details).

The strong magnification events are transient, because the source, the lensing galaxy and the microlensing centres in the galaxy are moving with respect to each other. The relative velocity of the source with respect to the lens is composed of the contributions from the motions of all objects involved. The velocity of the Sun with respect to the cosmic microwave background reference frame is $v_{\text{obs}} \simeq 300$ km s⁻¹ in the direction at an angle $\simeq 106^\circ$ with respect to the direction towards PKS 1830-211 (ref. 30). Assuming that velocities of the lens, v_L , and the source,

v_S , are of the same order, one finds $v_{\text{rel}} \sim 10^3$ km s⁻¹. The relative velocity determines the timescale of the strong magnification, $t_{\text{cc}} = R_\gamma/v_{\text{rel}} \simeq 0.3(R_\gamma/10^{15}$ cm) yr. The detected changes of μ_γ occur already on the timescale of the flare repetition time τ_{rep} (see Supplementary Information), implying that $t_{\text{cc}} \lesssim \tau_{\text{rep}}$. This limits the source size to be $R_\gamma \lesssim t_{\text{cc}}v_{\text{rel}} \simeq 6 \times 10^{14}(t_{\text{cc}}/0.2$ yr) cm. In the particular case of blazars, the source could be a blob in the jet moving with projected velocity $v_s \sim c$. If this is the case, the constraint from the caustic crossing timescale becomes much weaker than the constraint imposed by the maximal magnification ratio.

The mass of the lensing galaxy can be estimated from the observed size of the Einstein ring $R_{E,\text{gal}} = \theta_E D_L \simeq 4$ kpc. This gives $M_{\text{gal}} \sim 10^{11}M_\odot$ within $R_{E,\text{gal}}$ —that is, a galaxy similar to the Milky Way. The surface density of stars in the galaxy is only about $\Sigma_{\text{gal}} \sim 1M_\odot/\pi(R_E^*)^2$, assuming that the galactic mass within R_E is dominated by the luminous matter component. The microlensing events follow each other on the timescale $T \sim \sqrt{M_*/\Sigma_{\text{gal}}}/v_{\text{rel}} \simeq 10(M_*/M_\odot)^{1/2}(v/10^3$ km s⁻¹)⁻¹ yr. We argue that the caustic crossing events are responsible for the observational appearance of the strong flares of PKS 1830-211. Indeed, large, up to an order of magnitude, increases of the source flux during the flares are mostly caused by the large magnification factor in one of the images. The observed difference in the magnification factors

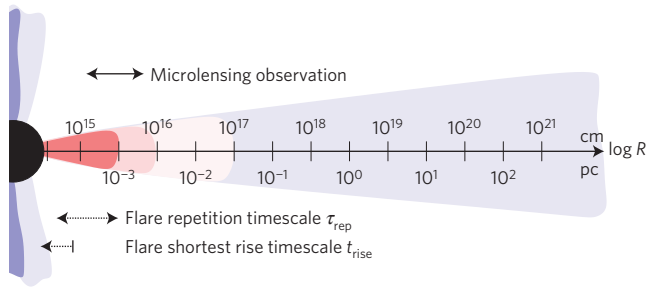


Figure 2 | Summary of constraints on the size of the γ -ray emission zone of PKS 1830-211, compared to its characteristic distance scale. The range of the source sizes constrained by the detection of microlensing is based on our simulation of the caustic patterns, described in Supplementary Information. Constraints based on the flare repetition timescale τ_{rep} and flare rise time t_{rise} are less direct and are thus indicated with the dashed arrows. The constraint based on the t_{rise} was computed under the assumption of a stationary source and does not include the correction for the uncertain Doppler factor of the jet. The colour coding along the coordinate axis represents the putative location of the γ -ray emission region (red) and the typical sizes of the accretion flow (pink), broad line region (light pink) and jet (light blue).

μ_γ between the separate sub-flares of a single flaring episode (for example, μ_γ changes from 6.5 ± 1.5 to 2.4 ± 0.5 during the brightest flaring episode) confirms this assumption.

To verify the conclusion on the influence of microlensing on the source variability and on the small source size R_γ , we have performed simulations of microlensing caustics maps produced taking into account the surface mass density of the lensing galaxy (see Supplementary Information for details). We find that at least one magnification event with $\mu_\gamma \sim 2-7$ is expected for a very compact source with extension $R_\gamma \approx (1-10) \times 10^{15}$ cm, consistent with our estimate based on the caustic crossing timescale τ_{cc} , as well as the simplified analytical estimate, given above.

The intrinsic source variability is characterized by the timescale $\tau_{\text{rep}} \approx 76$ d, which could be associated with the repetition rate of the sub-flares in each flaring (or caustic crossing) episode. The multiples of τ_{rep} also correspond to the intervals between the flaring episodes (see Supplementary Information for the detailed information). There are, in total, seven sub-flares in the four flaring episodes detected within the light curve of the source. Splitting the entire observation time span into ~ 25 d bins, corresponding to the duration of the sub-flares, one finds that the chance coincidence probability for the sub-flares to fall into time bins spaced by multiples of the 76 d interval is less than 1%.

Although the exact origin of the repetition timescale τ_{rep} can not be firmly established, its possible interpretation is that it is associated with the quasi-periodicity of the signal. Tentatively associating τ_{rep} with the period of rotation over a Keplerian orbit, one finds that the size of the orbit is $R_\gamma \approx 2 \times 10^{15} (\tau_{\text{rep}}/76 \text{ d})^{2/3} (M_{\text{BH}}/10^9 M_\odot)^{1/3}$ cm.

Another complementary estimate of the emission region size can be derived from the minimal variability timescale of the γ -ray emission. The time dependence of the particularly fast variable episode around MJD 55484.5 is fitted well with an exponential rise/decay profile, with the e -folding rise/decay timescales being $t_{\text{rise}} = 0.49 \pm 0.15$ d and $t_{\text{decay}} = 1.2 \pm 0.2$ d (see Supplementary Information for details). The rise timescale corresponds to the light-crossing time of the region of the size $R_\gamma < ct_{\text{rise}}/(1+z_s) \approx 10^{15}$ cm. This constraint should be corrected by the bulk Doppler factor of the jet if the emission is produced in the relativistic jet aligned along the line of sight. A summary of all constraints on the γ -ray source size derived from the intrinsic variability and microlensing timescales is given in Fig. 2.

Contrary to the γ -ray light curve, the X-ray light curve of the source does not reveal the signatures of the gravitational microlensing (see Fig. 2 of the Supplementary Information). The X-ray flux measured by SWIFT/XRT during the MJD 55550–55600 interval is consistent within $\sim 10\%$ with the previous measurements of the flux, spanning over almost a decade. The same is true for the hard X-ray flux monitored by INTEGRAL and SWIFT/BAT. Thus, the possibility of strong magnification by a factor $\mu_X \approx \mu_\gamma$ due to microlensing in the X-ray band is ruled out. This imposes a constraint on the (hard)X-ray source size of $R_X \gtrsim R_E^* \approx 4 \times 10^{16}$ cm.

PKS 1830-211 is one of the most powerful known blazars, with a luminosity $L \sim 3 \times 10^{48} \mu^{-1} \Gamma^{-2} \text{ erg s}^{-1}$, where $\mu \sim 10$ is the overall magnification factor and $\Gamma \sim 10$ is the bulk Lorentz factor of the jet (both uncertain). Such a luminosity corresponds to the Eddington luminosity $L_{\text{Edd}} \approx 10^{47} (M_{\text{BH}}/10^9 M_\odot) \text{ erg s}^{-1}$ of a black hole of mass $M_{\text{BH}} \sim 10^8-10^9 M_\odot$ and size $2R_{\text{BH}} \approx 10^{14}-10^{15}$ cm. The size of the AGN ‘central engine’ in PKS 1830-211 is comparable to the projected γ -ray source size derived above. The deprojected size of the γ -ray emitting part of the jet could be $\sim \Gamma$ times larger. Still, the γ -ray emission is produced in a very compact source, at most $\sim 10-100$ times larger than the black hole size.

Our analysis constrains the size, but not directly the location of the γ -ray emission region. However, typical linear scales of structures in the AGN jet with opening angle Θ_{jet} grow as $R\Theta_{\text{jet}}$ with the distance R from the black hole. This indicates that the γ -ray emission region should be situated in the vicinity of the black hole, rather than in the parsec-scale jet. The possibility that small sub-structures in the parsec-scale jet dominate the γ -ray signal is also disfavoured by the data (see Supplementary Information for details).

Detection of the extremely compact size of the γ -ray source poses a conventional problem for the escape of γ -rays. The essence of the problem is that γ -rays with energy E_γ larger than $E_{\text{thr}} = 2(m_e c^2)^2 / (\epsilon(1+z_s)^2) \sim 4 \times 10^7 (\epsilon/1 \text{ keV})^{-1} \text{ eV}$ produce e^+e^- pairs in collisions with the soft background photons of energy ϵ . The low-energy photons, contributing to the pair production opacity of the source, could either originate from the accretion flow onto the black hole or be a part of the overall emission from the AGN jet. In the latter case, the pair production threshold has to be corrected by taking into account that the collision angle $\alpha \sim \Gamma^{-1}$, so that $E_{\text{thr}} \approx 10^8 \Gamma^2 (\epsilon/1 \text{ keV})^{-1} \text{ eV}$.

The constraint $R_X \gtrsim R_E^* \approx 4 \times 10^{16}$ cm on the size of the X-ray emission region implies the optical depth with respect to pair production is $\tau \lesssim 3$. Thus, γ -rays with energies $E_\gamma \sim 10$ GeV are able to escape from the source (see Supplementary Information for the detailed calculation).

The accretion flow onto the black hole mainly produces radiation in the visible and ultraviolet band (forming the so-called ‘big blue bump’ in the source spectrum). The energy of the visible–ultraviolet photons, 1–30 eV, is too low to affect the source flux in the observed range of γ -ray energies, $E \leq 30$ GeV. Similar conclusions can be reached for the synchrotron photons, spanning the even lower energy range $10^{-5} \text{ eV} \leq \epsilon \leq 1 \text{ eV}$. Thus, the condition that the source should be at most moderately opaque with respect to the $\gamma\gamma$ pair production does not contradict the measurement of the compact size of the γ -ray emission region of PKS 1830-211.

The measurement of the extremely compact size of the γ -ray source in PKS 1830-211, reported here, removes the long-standing uncertainty of the location of the AGN γ -ray emitting zone (see Fig. 2). GeV band γ -ray emission is produced at the base of the jet, at a distance no greater than 10–100 times the Schwarzschild radius of the supermassive black hole powering the emission. The γ -ray emission dominates the energy output of the formation/collimation region of the jet. This implies that the particle acceleration process is an essential element of the (uncertain) physical mechanism at play in the generation of jets by supermassive black holes.

Received 17 October 2014; accepted 25 May 2015;
published online 6 July 2015

References

- Urry, C. M. & Padovani, P. Unified schemes for radio-loud active galactic nuclei. *Publ. Astron. Soc. Pac.* **107**, 803–845 (1995).
- Aharonian, F. *et al.* An exceptional very high energy γ -ray flare of PKS 2155-304. *Astrophys. J.* **664**, L71–L74 (2007).
- Vovk, I. & Neronov, A. Variability of γ -ray emission from blazars on black hole timescales. *Astrophys. J.* **767**, 103 (2013).
- Abdo, A. A. *et al.* A change in the optical polarization associated with a γ -ray flare in the blazar 3C279. *Nature* **463**, 919–923 (2010).
- Tavecchio, F. *et al.* On the origin of the γ -ray emission from the flaring blazar PKS 1222+216. *Astron. Astrophys.* **534**, A86 (2011).
- Ghisellini, G., Tavecchio, F., Foschini, L., Bonnoli, G. & Tagliaferri, G. The red blazar PMN J2345-1555 becomes blue. *Mon. Not. R. Astron. Soc.* **432**, L66 (2013).
- Nolan, P. L. *et al.* Fermi large area telescope second source catalog. *Astrophys. J.* **199**, 31 (2012).
- Jelley, J. V. Absorption of high-energy γ -rays within quasars and other radio sources. *Nature* **211**, 472–475 (1966).
- Maraschi, L., Ghisellini, G. & Celotti, A. A jet model for the γ -ray emitting blazar 3C 279. *Astrophys. J.* **397**, L5–L9 (1992).
- Dermer, C. D., Schlickeiser, R. & Mastichiadis, A. High-energy γ radiation from extragalactic radio sources. *Astrophys. J.* **256**, L27–L30 (1992).
- Bednarek, W. Can high-energy γ -ray photons escape from the radiation field emitted by an accretion disk? *Astron. Astrophys.* **278**, 307–314 (1993).
- Liu, H. T. & Bai, J. M. Absorption of 10–200 GeV γ rays by radiation from broad-line regions in blazars. *Astrophys. J.* **653**, 1089–1097 (2006).
- Poutanen, J. & Stern, B. GeV Breaks in blazars as a result of γ -ray absorption within the broad-line region. *Astrophys. J.* **717**, L118–L121 (2010).
- Begelman, M. C., Fabian, A. C. & Rees, M. J. Implications of very rapid TeV variability in blazars. *Mon. Not. R. Astron. Soc.* **384**, L19–L23 (2008).
- Giannios, D., Uzdensky, D. A. & Begelman, M. C. Fast TeV variability in blazars: Jets in a jet. *Mon. Not. R. Astron. Soc.* **395**, L29–L33 (2009).
- Barkov, M. V., Aharonian, F. A., Bogovalov, S. V., Kelner, S. R. & Khangulyan, D. Rapid TeV variability in blazars as a result of jet–star interaction. *Astrophys. J.* **749**, 119 (2012).
- Mediavilla, E., Jimenez-Vicente, J., Munoz, J. A., Mediavilla, T. & Ariza, O. Statistics of microlensing caustic crossings in Q 2237+0305: Peculiar velocity of the lens galaxy and accretion disk size. *Astrophys. J.* **798**, 138 (2015).
- Guerras, E. *et al.* Microlensing of quasar ultraviolet iron emission. *Astrophys. J.* **778**, 123 (2013).
- Kochanek, C. S. Quantitative interpretation of quasar microlensing light curves. *Astrophys. J.* **605**, 58–77 (2004).
- Eigenbrod, A. *et al.* Microlensing variability in the gravitationally lensed quasar QSO 2237+0305 = the Einstein Cross. II. Energy profile of the accretion disk. *Astron. Astrophys.* **490**, 933–943 (2008).
- Chartas, G. *et al.* Revealing the structure of an accretion disk through energy-dependent X-ray microlensing. *Astrophys. J.* **757**, 137 (2012).
- Jauncey, D. L. *et al.* An unusually strong Einstein ring in the radio source PKS1830-211. *Nature* **352**, 132–134 (1991).
- Lidman, C. *et al.* The redshift of the gravitationally lensed radio source PKS 1830-211. *Astrophys. J.* **514**, L57–L60 (1999).
- Wiklind, T. & Combes, F. The redshift of the gravitational lens of PKS1830-211 determined from molecular absorption lines. *Nature* **379**, 139–141 (1996).
- Lovell, J. E. J. *et al.* PKS 1830-211: A possible compound gravitational lens. *Astrophys. J.* **472**, L5–L7 (1996).
- Cheung, C. C. *et al.* Fermi Large Area Telescope detection of gravitational lens delayed?—Ray flares from blazar B0218+357. *Astrophys. J.* **782**, L14 (2014).
- Abdo, A. A. *et al.* γ -ray flaring activity from the gravitationally lensed blazar PKS 1830-211 observed by Fermi LAT. *Astrophys. J.* **799**, 143 (2015).
- Lovell, J. E. J. *et al.* The time delay in the gravitational lens PKS 1830-211. *Astrophys. J.* **508**, L51–L54 (1998).
- Chang, K. Maximum flux amplification by star disturbances in gravitational lens galaxies. *Astron. Astrophys.* **130**, 157–161 (1984).
- Kogut, A. *et al.* Dipole anisotropy in the COBE differential microwave radiometers first-year sky maps. *Astrophys. J.* **419**, 1–6 (1993).

Acknowledgements

The work of I.V. is supported by the Swiss National Science Foundation grant P2GEP2_151815. The work of A.N. is supported by the Swiss National Science Foundation grant PP00P2_144923.

Author contributions

I.V. and D.M. performed the analysis of the Fermi/LAT data. A.N. and I.V. jointly investigated the theoretical aspects of this work. D.M. performed the analysis of the INTERGRAL observations. A.N. and I.V. jointly wrote the paper. All authors took part in discussion of the results and contributed to the manuscript.

Additional information

Supplementary information is available in the [online version of the paper](#). Reprints and permissions information is available online at www.nature.com/reprints. Correspondence and requests for materials should be addressed to A.N. or I.V.

Competing financial interests

The authors declare no competing financial interests.